

# Comparison of Snow Water Equivalent Estimated in Central Japan by High-Resolution Simulations Using Different Land-Surface Models

Masatoshi Kuribayashi<sup>1</sup>, Nam Jin Noh<sup>1</sup>, Taku M. Saitoh<sup>1</sup>, Ichiro Tamagawa<sup>1</sup>,  
Yasutaka Wakazuki<sup>2</sup>, and Hiroyuki Muraoka<sup>1</sup>

<sup>1</sup>River Basin Research Center, Gifu University, Gifu, Japan

<sup>2</sup>Center for Research in Isotopes and Environmental Dynamics, University of Tsukuba, Tsukuba, Japan

## Abstract

We estimated the snow water equivalent (SWE) of snowpack in central Japan from September 2006 to August 2008 by using a 3.3 km-mesh regional climate model with two land-surface models: Noah land-surface model (Noah LSM), and Noah land-surface model with multiparameterization options (Noah MP). The model validation for temporal variations of SWE at the Tohkamachi station and the comparison of modeled maximum SWE with estimated that from observed maximum snow depth at ten sites showed that Noah MP could simulate spatiotemporal variations of SWE better than Noah LSM which underestimated SWE. Simulated SWE in central Japan peaked in March, but the difference of SWE between the two land-surface models was greatest in April. SWE determined using Noah LSM (Noah MP) in analysis domain reached 18.1% (28.5%) of the total storage capacity of high dams in Japan in March 2007, whereas it reached 32.4% (44.1%) in March 2008. The difference of SWE between the two land-surface models was particularly high under warm conditions, that is, during the snowmelt season, and during a warmer than normal winter. Our results indicate that the choice of land-surface model for estimates of SWE is important under warm climatic conditions.

**(Citation:** Kuribayashi, M., N. J. Noh, T. M. Saitoh, I. Tamagawa, Y. Wakazuki, and H. Muraoka, 2013: Comparison of snow water equivalent estimated in central Japan by high-resolution simulations using different land-surface models. *SOLA*, 9, 148–152, doi:10.2151/sola.2013-033.)

## 1. Introduction

The amount of winter snowfall in mountainous areas of central Japan is greater than most other mountainous regions in the world. The snowpack in central Japan provides plentiful water resources during the snowmelt season, and functions as a natural reservoir for the rest of the year. The water resources derived from snowpack can be calculated as snow water equivalent (SWE). The spatial distribution of SWE can be estimated by means of integration analysis using in-situ observations, satellite observations, and snow model (Asaoka et al., 2007). However, the estimated SWE is temporally discontinuous, and its accuracy in mountainous areas of central Japan is not reliable enough because there are few meteorological observation stations in these areas.

Climate models provide an effective method to evaluate spatiotemporal variations of SWE. For example, Hosaka et al. (2005) estimated global SWE by using a 20 km-mesh atmospheric general circulation model. However, their study did not provide quantitative estimates of SWE in Japan, and the spatial resolution of the model was too coarse to simulate the meso-scale cumulus cloud systems that form over the Sea of Japan in winter. To date, there have been no quantitative estimations of SWE obtained in mountainous areas of central Japan using a high-resolution model with a spatial grid of less than 5 km.

Regional climate simulations obtained by the dynamical downscaling method with a regional climate model to calculate snow depth ( $h_s$ ) in Japan have reported that rising air temperature causes a reduction of  $h_s$  at low altitude (Hara et al. 2008; Kawase et al. 2012). These simulations used the Noah land-surface model (Noah LSM; Chen and Dudhia 2001). However, Livneh et al. (2010) reported that the Noah LSM underestimates SWE in early spring because of incomplete algorithms for the decay of snow albedo associated with snowpack aging and the refreezing of snowmelt water within the snowpack. Additionally, it described that developing a multilayer snow model to capture metamorphism of snow and intrasnow heat exchange would be able to provide immediate improvements in simulations. Niu et al. (2011) reported that the Noah land-surface model with multiparameterization options (Noah MP; Niu et al. 2011), which can consider a three-layer snowpack, provides better estimates of observed  $h_s$ , snow density ( $\rho_s$ ), and SWE than the Noah LSM. Nevertheless, the performance of Noah MP to simulate snowpack has not been validated in heavy-snowfall area in Japan.

The purposes of this study are to quantitatively evaluate SWE in mountainous areas of central Japan using a high-resolution model, and to clarify the effect on calculated SWE of the choice of land-surface model for each month. In this study, we compared SWE simulated in central Japan from September 2006 to August 2008 by a 3.3 km-mesh regional climate model used with either Noah LSM or Noah MP, and discussed about the characteristics of difference of SWE simulated for the two land-surface models.

## 2. Observation data and model description

### 2.1 Observation data

We used precipitation and  $h_s$  data recorded by the Automated Meteorological Data Acquisition System of the Japan Meteorological Agency (JMA) and the water quality database of the Ministry of Land, Infrastructure, Transport and Tourism (MLIT water information system). We used rain gauge data only from gauges with heating systems to screen out abnormal values caused by winter snowfall. In addition, we used meteorological data and snow pit data from the Tohkamachi field station of the Forestry and Forest Product Research Institute (FFPRI). Daily observations of SWE were made at 0900 JST at the Tohkamachi field station by using a snow sampler and platform scale (Takeuchi et al. 2009). Furthermore, we used precipitation and  $h_s$  data from the Takayama field station of Gifu University. Hourly observations of  $h_s$  were made by using an ultrasonic snow depth meter, excluding Takayama field station at which daily  $h_s$  data were made by snow scale. The locations and elevations of the sites recording  $h_s$  data are provided in Table 1 and Fig. 1a.

Concerning the climatic characteristics of target years, the anomalies of seasonal mean air temperature from December 2006 to February 2007, from March to May 2007, from December 2007 to February 2008, and from March to May 2008, were +1.32, +0.07, -0.09, and +0.42°C, respectively (JMA 2013).

### 2.2 Numerical simulation

Numerical simulations were done using the Weather Research and Forecasting (WRF) modeling system version 3.4.1 (Skamarock et al. 2008), which is a non-hydrostatic cloud-resolving nu-

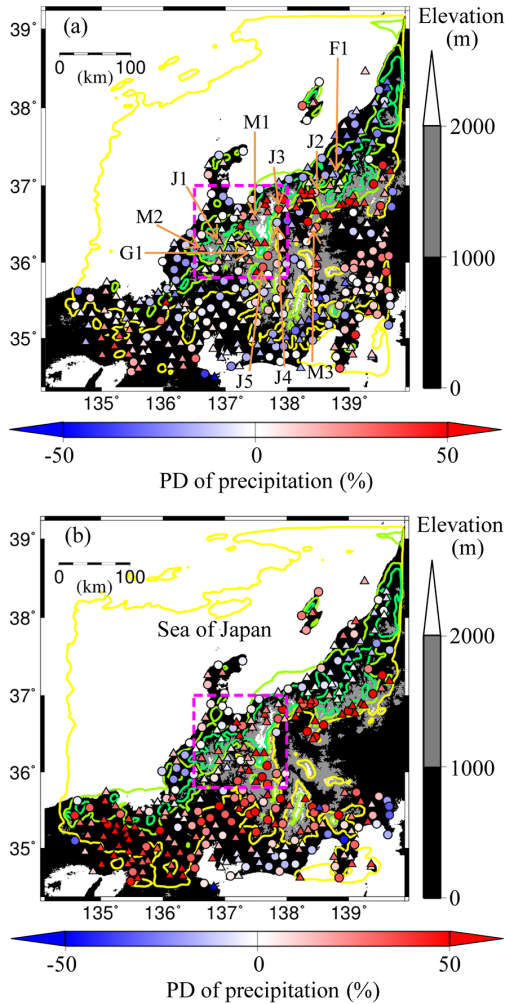


Fig. 1. Spatial distributions of percentage difference (PD, defined in Section 3.1) of modeled and observed cumulative precipitation (a) from 1 November 2006 to 31 March 2007, and (b) from 1 November 2007 to 31 March 2008. Modeled data shown only for simulation using Noah MP. Observed cumulative precipitation shown only for sites that recorded more than 250 mm. Rain gauge locations shown as circles (with wind shield) and triangles (without wind shield). Yellow, light green, and dark green contours show simulated cumulative precipitation of 500, 1000, and 1500 mm, respectively. The rectangle (purple dashed lines) indicates the analysis domain of Fig. 4. The annotated IDs with orange arrows indicate the observation stations provided in Table 1.

merical model. The computational domain (Fig. 1) was a gridded area of  $148 \times 160$  cells with a horizontal grid spacing of 3.3 km. The upper boundary of the model was the 50 hPa level and 42 vertical sigma levels were used. Time integration was continuous from 1 September 2006 to 31 August 2008. Initial and boundary conditions were based on JMA meso-scale analysis data (atmosphere), National Center for Environmental Prediction (NCEP)

Table 1. Locations and elevations of the observation stations recording snow depth.

ID	Data provider	Site name	Altitude (m a.s.l.)	Longitude ( $^{\circ}$ E)	Latitude ( $^{\circ}$ N)
F1	FFPRI	Tohkamachi	200	138.767	37.133
M1	MLIT	Senjugahara	474	137.446	36.582
J1	JMA	Shirakawa	478	136.897	36.273
M2	MLIT	Kazarashi	510	136.632	36.168
J2	JMA	Nozawaonsen	576	138.442	36.912
J3	JMA	Hakuba	703	137.862	36.698
J4	JMA	Ohmachi	784	137.833	36.523
J5	JMA	Kaidakougen	1130	137.602	35.938
G1	Gifu Univ.	Takayama	1342	137.422	36.142
M3	MLIT	Jizoutouge	1713	138.421	36.429

Table 2. Physics of the WRF model used for numerical simulations of SWE (other than the land surface model).

	Physics	References
Microphysics	WRF single moment 6-class microphysics scheme	Hong and Lim (2006)
Radiation (longwave)	Rapid Radiative Transfer Model	Mlawer et al. (1997)
Radiation (shortwave)	Dudhia	Dudhia (1989)
Boundary layer process	Mellor-Yamada, Nakanishi and Niino level 2.5	Nakanishi and Niino (2004)
Surface layer process	Mellor-Yamada, Nakanishi and Niino surface layer scheme	Nakanishi and Niino (2004)

final analysis data (land surface), and NCEP real-time global sea surface temperature analysis data (sea surface). For land use, we used 20-category MODIS data. References for the main physical processes in our simulation are provided in Table 2. We did not use cumulus parameterization options because the horizontal grid interval we used was fine enough to resolve the well-developed snow band above the Sea of Japan in winter (Murakami et al. 2003).

We performed simulations using two land-surface models, the Noah LSM (LSM-run hereafter) and the Noah MP (MP-run hereafter). Each land surface model was coupled on-line to atmosphere modeling. Koren et al. (1999) described parameterization for the calculation of SWE, snowmelt rate, and  $\rho_s$ . It reported that an upper limit of  $0.4 \text{ g cm}^{-3}$  was applicable for  $\rho_s$  in the Noah LSM, but there is no upper limit for  $\rho_s$  in the Noah MP. An important difference of the Noah MP is that it can consider a three-layer snowpack (depending on total  $h_s$ ), whereas Noah LSM treats the snowpack as a single layer. In addition, different options can be selected for various physical processes for simulation using Noah MP, while these physical processes are fixed for simulation using Noah LSM. Table 3 shows our selections for the major physical processes for calculating SWE in MP-run, compared with those in LSM-run. Other differences between the Noah LSM and the Noah MP and the detailed structure of the Noah MP are explained by Niu et al. (2011).

Table 3. Comparison of major options for SWE simulations using Noah LSM and Noah MP.

Options	Noah LSM	Noah MP
Surface exchange coefficient for heat	Chen97 (Chen et al. 1997)	Monin-Obukhov similarity theory (Brutsaert 1982)
Frozen soil permeability	Koren99 (Koren et al. 1999)	NY06 (Niu and Yang 2006)
Vegetation canopy layer	Combined surface layer of vegetation and ground surface	Separated the canopy layer from the ground surface
Radiation transfer through the vegetation canopy	Off	Modified two-stream scheme (Niu et al. 2011)
Snow surface albedo	Ek et al. (2003)	BATS (Yang et al. 1997)
Partitioning precipitation into rainfall and snowfall	Jordan (1991)	Jordan (1991)

### 3. Results and discussion

#### 3.1 Model validation for precipitation in the cold season

Because snowfall is the input to the snowpack, we validated the modeled precipitation for the cold season. The spatial distribution of the percentage difference (PD) of modeled to observed cumulative precipitation from 1 November to 31 March is shown in Fig. 1. PD was defined as

$$PD = \frac{P_m - P_o}{P_o} \times 100, \quad (1)$$

where  $P_m$  and  $P_o$  are modeled and observed cumulative precipitation, respectively. Figure 1 shows only  $P_m$  from the MP-run, because  $P_m$  values obtained from both runs were almost the same.  $P_m$  on the Sea of Japan side was about 1000 mm over the five cold months in the lowland area (< 1000 m a.s.l.), and  $P_m$  was more than 1500 mm in the mountainous area facing to the Sea of Japan (Fig. 1). Focusing on the lowland area on the Sea of Japan side, in 2006/2007 and 2007/2008, 73% and 78%, respectively, of observation sites showed absolute PD values of less than 20%. However, the model greatly overestimated precipitation in the highland area ( $\geq 1000$  m a.s.l.) for both years (Fig. 1 and Supplement 1).

There are three possible reasons for this overestimation. First, the elevations of mountain ridges were underestimated in the model because the 3.3 km grid was not fine enough to resolve the mountainous topography. Therefore, cumulus formed above the Sea of Japan would be modeled as flowing too far inland, reaching the area where many of the observation sites are above 1000 m elevation. Second, the 3.3 km grid was not fine enough to resolve micro-scale convective clouds and narrow snow band (Murakami et al. 2003); thus, water that should be precipitated from small cumulus over the lowlands on the Sea of Japan side of the study area would be modeled as falling in the mountainous area. Third, under-recording of precipitation by rain gauges is much higher for snow than for rain, and increases with increasing wind speed even when there is a wind shield installed (Larson and Peck 1974). Thus, precipitation recorded under windy conditions may have been erroneously low.

#### 3.2 Temporal variations of snowpack at Tohkamachi field station

Comparison of the temporal variations of simulated and observed cumulative precipitation, cumulative snowfall,  $h_s$ ,  $\rho_s$ , SWE, and air temperature at the Tohkamachi field station (Fig. 2) showed that, although both land-surface models underestimated precipitation, reproducibility of the observed data was better for 2007/2008 than for 2006/2007. Underestimation of precipitation for 2006/2007 might have contributed to underestimation of  $h_s$  and SWE for 2006/2007 (Figs. 2a, b, c), since it could result in underestimation of snowfall. Snowfall of the LSM-run was almost same with that of the MP-run as with precipitation (Fig. 2a). Simulated  $h_s$  and SWE from the MP-run for 2007/2008 were relatively consistent with observed values, but were substantially underestimated for the LSM-run for the snow season of 2007/2008 (Figs. 2b, c). Simulated  $\rho_s$  from the MP-run for 2007/2008 reproduced well the observed data, whereas  $\rho_s$  from the LSM-run reached a maximum of  $0.4 \text{ g cm}^{-3}$ , below the observed value after day of year (DOY) 70 in 2008 (Fig. 2b). Both observed and simulated  $\rho_s$  were defined as the SWE divided by the  $h_s$  to compare the averages of  $\rho_s$  over all snow depths.

When we focus on DOY 50–70 in 2008, the observed SWE increased despite a concurrent slight reduction of observed  $h_s$ , indicating that snowfall during this period increased SWE, but a rapid increase of  $\rho_s$  restricted the increase of  $h_s$  (Figs. 2a, b, c). The MP-run captured these temporal variations to some extent, but the LSM-run did not. Judging from the temporal variations of SWE and air temperature, the snowmelt rate of the LSM-run was greater than those of both the observed data and the MP-run when the daily mean air temperature was around  $0^\circ\text{C}$  during DOY 1–70 of 2008 (Figs. 2c, d). That is, the MP-run could reproduce the snowmelt rate better than the LSM-run when daily mean air

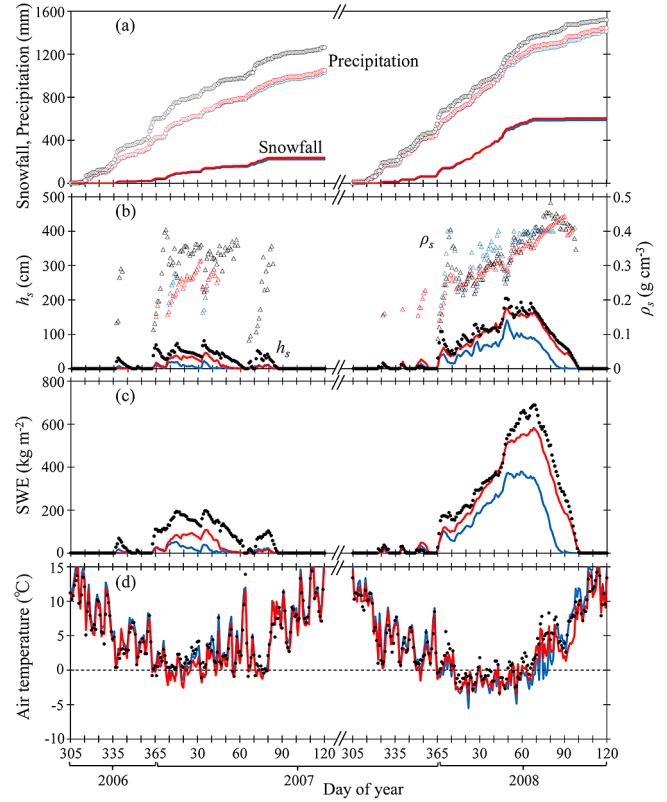


Fig. 2. Time series at Tohkamachi field station of modeled and observed (a) cumulative precipitation and cumulative snowfall, (b) snow depth ( $h_s$ ) and snow density ( $\rho_s$ ), (c) snow water equivalent (SWE), and (d) daily mean air temperature (2 m above ground). Precipitation is the sum of snowfall and rainfall, but observed precipitation is not classified into snowfall or rainfall. Colors of symbols and lines indicate observed data (black) and simulated data from MP-run (red) and LSM-run (blue).

temperatures were around  $0^\circ\text{C}$ , and it resulted in the widening differences of  $h_s$  and SWE between the LSM-run and the MP-run.

One of the possible reasons for the better reproducibility of MP-run is that Noah MP consider the retention of snowmelt water at midday hours and refreezing of the liquid water within snowpack at nighttime (Niu et al. 2011). However, this phenomenon is unlikely at Tohkamachi field station, because both the observed snow temperature and the simulated one by MP-run were almost  $0^\circ\text{C}$  at every snow layer even in midwinter. That is, significant refreezing could not happen. Other possible reasons are the differences on how to calculate surface exchange coefficient for heat, radiation transfer through the vegetation canopy, snow surface albedo, and so on (Table 3). The sensitivity of each parameter to simulate SWE should be evaluated more carefully in future studies.

#### 3.3 Quantitative estimations of SWE in central Japan

The relationship between maximum  $h_s$  ( $h_{s, \text{max}}$ ) and maximum SWE ( $\text{SWE}_{\text{max}}$ ) was formulated by Eq. (2), by using long-term observation data at some sites located in mountainous areas of Japan by the National Research Institute for Earth Science and Disaster Prevention (Yamaguchi et al. 2011).

$$\text{SWE}_{\text{max}} = 272 \times \left( \frac{h_{s, \text{max}}}{100} \right)^{1.3}, \quad (2)$$

Using the Eq. (2) and the observed  $h_{s, \text{max}}$  at ten representative sites shown in Table 1 and Fig. 1, we estimated the  $\text{SWE}_{\text{max}}$  for the winters of 2006/2007 and 2007/2008. Then, we compared the estimated and modeled  $\text{SWE}_{\text{max}}$  at these sites for each winter, and compared  $P_o$  and  $P_m$  from the MP-run as well (Fig. 3).  $\text{SWE}_{\text{max}}$

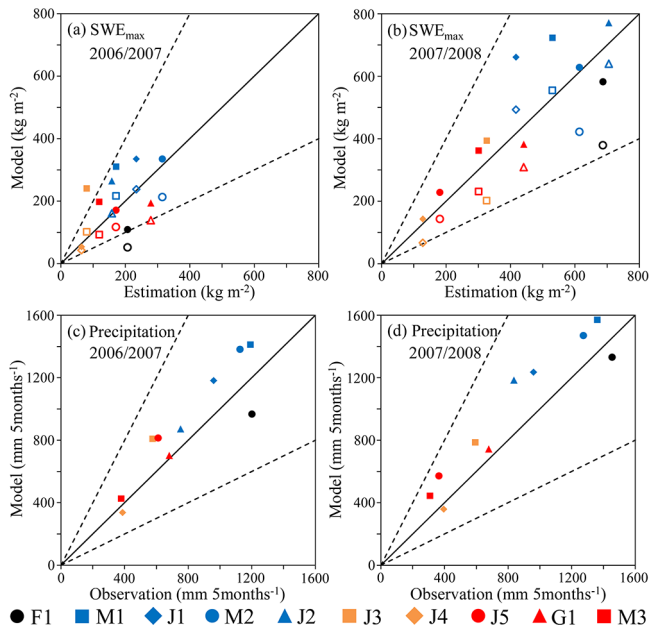


Fig. 3. Scatter plots of estimated versus modeled maximum snow water equivalent ( $SWE_{max}$ ) during the winter of (a) 2006/2007, and (b) 2007/2008. The equation to estimate  $SWE_{max}$  is shown in Section 3.3. Scatter plots of observed versus modeled cumulative precipitation (c) from 1 November 2006 to 31 March 2007, and (d) from 1 November 2007 to 31 March 2008. The solid and open symbols indicate MP-run and LSM-run, respectively. Color of symbols denotes the range of elevation in which each observation station is located: black, blue, orange, and red mean 0–400 m, 400–700 m, 700–1000 m, and above 1000 m, respectively (See Table 1 for detail locations and elevations). 1:1, 1:2, and 2:1 reference lines are shown.

from the LSM-run was smaller than that estimated from Eq. (2) except at M1, J1, and J2, whereas  $SWE_{max}$  from the MP-run was larger than the estimation except at F1, M2, J4, J5, and G1 (Figs. 3a, b). Considering that  $P_m$  was larger than  $P_o$  except at F1, J4, and G1 (Figs. 3c, d), the  $SWE_{max}$  from the MP-run could be more reasonable than those from the LSM-run. It indicates that Noah MP can simulate the spatial distribution of SWE better than Noah LSM if the model accuracy for winter precipitation was improved.

To avoid biases caused by the lateral boundary condition and the uncertainty of modeled precipitation, we set our analysis domain to an area where the reproducibility of observed cumulative precipitation during the cold season was relatively good (Fig. 1). We then simulated monthly SWE for both land-surface models for three ranges of elevation for the period from November 2006 to August 2008 (Fig. 4a). The land areas at altitude ranges of 0–1000 m, 1000–2000 m, and above 2000 m in this analysis domain were approximately 9958 km<sup>2</sup>, 6010 km<sup>2</sup>, and 629 km<sup>2</sup>, respectively. For both land-surface models, the total SWE simulated for the entire elevation range peaked in March. Comparison of SWE simulated for both land-surface models to the combined effective storage capacity of all of the high dams in Japan (17106 Mt; Japan Dam Foundation 2008) showed that for March 2007 the SWE simulated by Noah LSM (Noah MP) was 18.1% (28.5%) of high-dam capacity, whereas for March 2008 it was 32.4% (44.1%). The simulated spatial distributions of SWE in March 2007 and 2008 are shown in Supplement 2. The SWE per unit area was greater at higher altitudes (Supplement 2), although the SWE simulated at 1000–2000 m altitude accounted for more than half of the total SWE over the entire range of elevations during the period from January to May (Fig. 4a).

### 3.4 Differences of simulated SWE for Noah LSM and Noah MP

The monthly variations of the difference of SWE simulated for the two land-surface models (Fig. 4b) show that the differences of total SWE for the entire range of elevations were greatest in April

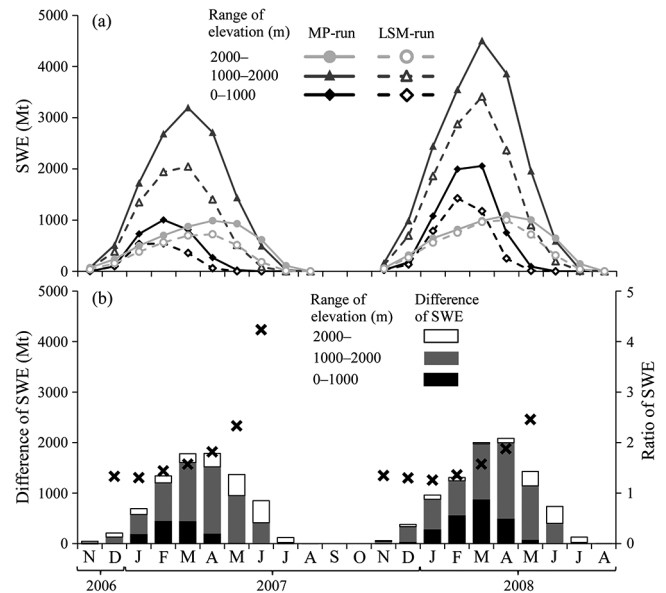


Fig. 4. (a) Seasonal variations of simulated snow water equivalent (SWE) for both land-surface models for three elevation ranges within the analysis domain shown in Fig. 1. (b) Seasonal variations of the differences of estimated SWE (MP-run minus LSM-run) for each elevation range and the ratio (crosses) of SWE (MP-run to LSM-run) over the entire elevation range.

of both years, although the differences in March were of similar magnitude to those in April. The differences of SWE for altitude ranges of 0–1000 m, 1000–2000 m, and above 2000 m peaked in March, April, and June, respectively (Fig. 4b). Thus, the peaks for SWE differences for each altitude range lagged behind the peaks of each SWE, and these lags were greater at higher altitudes (Fig. 4). This result reflects the widening of SWE difference for snowmelt season and the difference of the length of snowmelt season depending on altitude.

The total SWE of the MP-run was 1.66 (1.44) times that of the LSM-run during January to June of 2007 (2008), and the ratio of the total SWE of the MP-run to that of the LSM-run increased exponentially over that period (Fig. 4b). In the snow season of 2006/2007, which was a warm winter in Japan, this ratio was higher than that of the snow season of 2007/2008, which was a normal winter. Furthermore, the gradient of the exponential curve was considerably greater in 2006/2007 than in 2007/2008 (Fig. 4b). The higher ratio for the warm winter might reflect the high frequency of increases of air temperature to around 0°C, which is the temperature at which the greatest differences of SWE simulated with the two land-surface models were observed (see Section 3.2). This result indicates that the differences of simulated SWE for the two land-surface models would be greater under warm conditions.

## 4. Summary and conclusions

We estimated SWE in central Japan by using a 3.3 km-mesh WRF model with two land-surface models (Noah LSM and Noah MP). We then validated the performance of the model against observed data and compared the SWE values obtained for the two land-surface models. Comparison of the temporal variations of simulated and observed SWE at the Tohkamachi field station showed that Noah MP reproduced the observed SWE better than Noah LSM, which underestimated the observed SWE when daily mean air temperature was around 0°C. Comparison of modeled  $SWE_{max}$  with estimated that from observed  $h_{s,max}$  at ten representative sites indicated that Noah MP might simulate the spatial distribution of SWE better than Noah LSM.

SWE peaked in March for both land-surface models. For Noah LSM, total SWE in analysis domain reached 18.1% of the total storage capacity of high dams in Japan in 2007 and 32.4% in 2008. For Noah MP, these proportions were 28.5% in 2007 and 44.1% in 2008. Because the difference of total SWE for the two land-surface models increased during the snowmelt season, that difference was greatest in April of both years. The total SWE estimated using Noah MP was about 1.5 times larger than that for Noah LSM. The ratio of the total SWE estimated with Noah MP to that estimated with Noah LSM increased exponentially through the snow season, and was higher for the warm winter of 2006/2007 than for the normal winter of 2007/2008.

Our results indicate that the choice of land-surface model for estimations of SWE in central Japan is important under warm climatic conditions such as those during the snowmelt season and those of lowland areas. This choice is also important for predictions of the effects of global warming on snowpack. Further analyses similar to this study are needed to assess the uncertainties related to choice of land-surface model for future predictions of snowpack.

## Acknowledgements

We are grateful to Mr. K. Kurumado for providing observed  $h_s$  and precipitation data from Takayama field station. This research was supported by the Japanese Alps Inter-University Cooperative Project (JALPS) Fund of the Ministry of Education, Culture, Science and Technology (MEXT) of Japan, and the Next Generation World-Leading Researchers (NEXT Program, Principal Investigator Dr. H. Muraoka) Fund of the Japan Society for the Promotion of Science.

## Supplements

Supplement 1 describes the relationship of elevation to PD for cumulative precipitation. Supplement 2 describes the spatial distributions of SWE simulated using Noah LSM and Noah MP in March of 2007 and 2008.

## References

- Asaoka, Y., Y. Kominami, Y. Takeuchi, H. Daimura, and N. Tanaka, 2007: Estimation of snow water equivalent in wide area based on satellite remote sensing and regional characteristics of the snowmelt rate factor. *J. Japan Soc. Hydrol. & Water Resour.*, **20**, 519–529 (in Japanese).
- Brutsaert, W. A., 1982: *Evaporation Into the Atmosphere*. Reidel Publishing Company, 299 pp.
- Chen, F., and J. Dudhia, 2001: Coupling an advanced land surface–hydrology model with the Penn State–NCAR MM5 modeling system. Part I: Model implementation and sensitivity. *Mon. Wea. Rev.*, **129**, 569–585.
- Chen, F., Z. Janjic, and K. E. Mitchell, 1997: Impact of atmospheric surface-layer parameterizations in the new land-surface scheme of NCEP mesoscale Eta model. *Bound.-Layer Meteor.*, **85**, 391–421.
- Dudhia, J., 1989: Numerical study of convection observed during the winter monsoon experiment using a mesoscale two-dimensional model. *J. Atmos. Sci.*, **46**, 3077–3107.
- Ek, M. B., K. E. Mitchell, Y. Lin, E. Rogers, P. Grunmann, V. Koren, G. Gayno, and J. D. Tarpley, 2003: Implementation of Noah land surface model advances in the National Centers for Environmental Prediction operational mesoscale Eta model. *J. Geophys. Res.*, **108**, D22, 8851.
- Hara, M., T. Yoshikane, H. Kawase, and F. Kimura, 2008: Estimation of the impact of global warming on snow depth in Japan by the pseudo-global-warming method. *Hydrol. Res. Lett.*, **2**, 61–64.
- Hong, S., and J. J. Lim, 2006: The WRF single-moment 6-class microphysics scheme (WSM6). *J. Korean Meteor. Soc.*, **42**, 129–151.
- Hosaka, M., D. Nohara, and A. Kitoh, 2005: Changes in snow cover and snow water equivalent due to global warming simulated by a 20 km-mesh global atmospheric model. *SOLA*, **1**, 93–96.
- Japan Dam Foundation, 2008: *Dam Yearbook*. 1671 pp (in Japanese).
- Japan Meteorological Agency, 2013: Available at: [http://www.data.kishou.go.jp/climate/cpinfo/temp/list/ssn\\_jpn.html](http://www.data.kishou.go.jp/climate/cpinfo/temp/list/ssn_jpn.html) (accessed 2013.8.30) (in Japanese).
- Jordan, R., 1991: A one-dimensional temperature model for a snow cover: technical documentation for SNTherm.89. *U. S. Army Cold Regions Research and Engineering Laboratory Special Report 91-16*, 49 pp.
- Kawase, H., T. Yoshikane, M. Hara, M. Fujita, N. N. Ishizaki, F. Kimura, and H. Hatsushika, 2012: Downscaling of snow cover changes in the late 20th century using a past climate simulation method over central Japan. *SOLA*, **8**, 61–64.
- Koren, V., J. Schaake, K. Mitchell, Q. Y. Duan, F. Chen, and J. M. Baker, 1999: A parameterization of snowpack and frozen ground intended for NCEP weather and climate models. *J. Geophys. Res.*, **104**, 19569–19585.
- Larson, L. W., and E. L. Peck, 1974: Accuracy of precipitation measurements for hydrologic modeling. *Water Resour. Res.*, **10**, 857–863.
- Livneh, B., Y. Xia, K. E. Mitchell, M. B. Ek, and D. P. Lettenmaier, 2010: Noah LSM snow model diagnostics and enhancements. *J. Hydrometeorology*, **11**, 721–738.
- Ministry of Land, Infrastructure, Transport and Tourism, 2013: Available at: <http://www1.river.go.jp/> (accessed 2013.6.25) (in Japanese).
- Mlawer, E. J., S. J. Taubman, P. D. Brown, M. J. Iacono, and S. A. Clough, 1997: Radiative transfer for inhomogeneous atmosphere: RRTM, a validated correlated-k model for the longwave. *J. Geophys. Res.*, **102**, D14, 16663–16682.
- Murakami, M., Y. Yamada, T. Matsuo, K. Iwanami, J. D. Marwitz, and G. Gordon, 2003: The precipitation process in convective cells embedded in deep snow bands over the Sea of Japan. *J. Meteor. Soc. Japan*, **81**, 515–531.
- Nakanishi, M., and H. Niino, 2004: An improved Mellor–Yamada level-3 model with condensation physics: its design and verification. *Bound.-Layer Meteor.*, **112**, 1–31.
- Niu, G. Y., and Z. L. Yang, 2006: Effects of frozen soil on snowmelt runoff and soil water storage at a continental scale. *J. Hydrometeorology*, **7**, 937–952.
- Niu, G. Y., Z. L. Yang, K. E. Mitchell, F. Chen, M. B. Ek, M. Barlage, A. Kumar, K. Manning, D. Niyogi, E. Rosero, M. Tewari, and Y. Xia, 2011: The community Noah land surface model with multiparameterization options (Noah-MP): 1. Model description and evaluation with local-scale measurements. *J. Geophys. Res.*, **116**, D12109.
- Skamarock, W. C., J. B. Klemp, J. Dudhia, D. O. Gill, D. M. Barker, M. G. Duda, X. Y. Huang, W. Wang, and J. G. Powers, 2008: A description of the advanced research WRF version 3. *NCAR Technical Note -475*, 113 pp.
- Takeuchi, Y., Y. Endo, S. Niwano, and S. Murakami, 2009: Data of meteorology and snow pit observations at Tohkamachi in Niigata prefecture, Japan (VII) (2004–05 to 2008–09, five winter periods). *Bulletin of FFPRI*, **8**, 227–232 (in Japanese).
- Yamaguchi, S., O. Abe, S. Nakai, and A. Sato, 2011: Recent fluctuations of meteorological and snow conditions in Japanese mountains. *Ann. Glaciol.*, **52**, 209–215.
- Yang, Z. L., R. E. Dickinson, A. Robock, and K. Y. Vinnikov, 1997: Validation of the snow submodel of the Biosphere–Atmosphere Transfer Scheme with Russian snow cover and meteorological observation data. *J. Climate*, **10**, 353–373.